ACS APPLIED MATERIALS & INTERFACES

Research Article

www.acsami.org

Highly Regenerable Mussel-Inspired Fe_3O_4@Polydopamine-Ag Core–Shell Microspheres as Catalyst and Adsorbent for Methylene Blue Removal

Yijun Xie,[†,⊥] Bin Yan,[†,⊥] Haolan Xu,[‡] Jian Chen,[§] Qingxia Liu,[†] Yonghong Deng,*[,∥] and Hongbo Zeng*[,†]

[†]Department of Chemical and Materials Engineering, University of Alberta, Edmonton, Alberta T6G 2V4, Canada

[‡]Ian Wark Research Institute, University of South Australia, Mawson Lakes, SA 5095, Australia

[§]National Institute for Nanotechnology, National Research Council, Edmonton, Alberta T6G 2M9, Canada

[∥]School of Chemistry and Chemical Engineering, South China University of Technology, Guangzhou, 510640, People's Republic of China

Supporting Information

ABSTRACT: We report a facile method to synthesize Fe_3O_4@polydopamine (PDA)-Ag core–shell microspheres. Ag nanoparticles (NPs) are deposited on PDA surfaces via *in situ* reduction by mussel-inspired PDA layers. High catalytic activity and fast adsorption of a model dye methylene blue (MB) at different pH values are achieved mainly due to the presence of monodisperse Ag NPs and electrostatic interactions between PDA and MB. The as-prepared Fe_3O_4@PDA-Ag microspheres also show high cyclic stability (>27 cycles), good acid stability, and fast regeneration ability, which can be achieved efficiently within several minutes by using $NaBH_4$ as the desorption agent, showing great potentials in a wide range of applications.

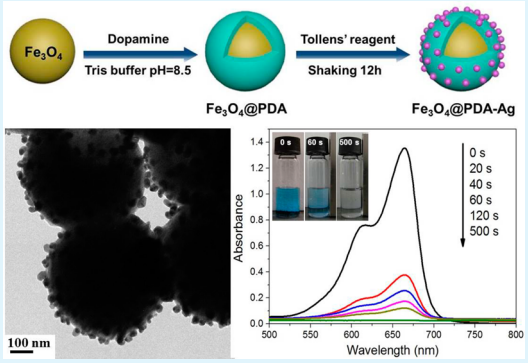

KEYWORDS: *Fe_3O_4@PDA-Ag microspheres, polydopamine, in situ reduction, fast adsorption, cyclic stability, regeneration ability, dye removal, water treatment*

1. INTRODUCTION

Water pollution by organic contaminants has become a serious environmental issue and received significant attention.[1,2] Among many organic pollutants, it is of special importance to solve the pollution challenges with organic dyes due to their wide applications in industries such as printing, textile, paper, paints, and plastics.[3,4] The immoderate release of wastewater containing organic dyes could impede sunlight penetration into water, thus reducing the photosynthetic reaction of plants; some synthetic dyes may cause severe health threats to human beings.[5,6] A variety of technologies have been exploited to remove these contaminants, such as adsorption, photocatalytic degradation, chemical oxidation, membrane filtration, flocculation, and electrooxidation.[4,7] Adsorption is one of the most effective approaches for the treatment of organic dyes and is commonly used due to its relatively low cost and easy operation.[8,9] Various kinds of adsorbents have been designed to remove the dyes in water with considerable adsorption capabilities, such as activated carbon,[10] carbon nanotubes,[11] graphene hydrogels,[2,12] and metal oxide.[6] Inspired by the unique wet adhesion capability of marine mussels, polydopamine (PDA) has attracted strong interest as a biomimetic polymer and a universal surface modification agent for various materials with a broad range of applications.[13,14] Recently, PDA-functionalized hybrid nanomaterials were developed as novel nanostructured adsorbents to remove organic dyes. Duan et al. reported a free-standing PDA-modified graphene hydrogel (PDA-GH) for water treatment.[12] Priestley et al. designed a novel core–shell adsorbent by converting Fe_3O_4@PDA into Fe_3O_4@C under thermal treatment for the adsorption of rhodamine B.[15] These adsorbents demonstrated good adsorption of organic dyes with the assistance of catechol groups of PDA or a hydrophobic carbon layer. Despite their considerable adsorption capabilities, many previously reported PDA-modified adsorbents and catalyst supports are limited by relatively long regeneration time or poor cyclic stability, which makes it challenging to recycle and reuse the adsorbents efficiently, further affecting their decontamination efficiencies in dye removal.

Herein, we present a facile synthetic method of *in situ* reduction to prepare core–shell Fe_3O_4@PDA-Ag microspheres, where polydopamine acts as both the reducing agent and the template for the formation of Ag nanoparticles (NPs) on the dopamine surfaces in one step.[16−18] It is well-known that

Received: March 18, 2014
Accepted: April 30, 2014
Published: April 30, 2014

   dx.doi.org/10.1021/am501632f | ACS Appl. Mater. Interfaces 2014, 6, 8845−8852

dopamine can spontaneously self-polymerize into polydopamine under mild solution conditions and form an adhesive coating layer on various substrates, as inspired by the unique underwater adhesion properties of marine mussel foot proteins.[13,14,16] Additionally, dopamine can serve as a reducing and capping agent to reduce noble metallic salts into metallic NPs.[15,16,19,20] Noble metal NPs are widely applied to the catalytic reduction of methylene blue (MB), a kind of common dye in the dye manufacturing industry, thanks to their high catalytic activity.[21,22] Thus, a facile route was developed in this work to synthesize novel Fe_3O_4@PDA-Ag core−shell microspheres with synergetic capabilities of high catalytic reduction activity and fast adsorption ability for MB at different pH values. The microspheres exhibit excellent cyclic performance via magnetic separation and a fast regeneration rate, which can be reused for more than 27 times by using $NaBH_4$ as the desorption agent, and each regeneration cycle requires only 6 min, revealing good potentials in practical applications.

2. EXPERIMENTAL SECTION

2.1. Materials. Anhydrous iron(III) chloride ($FeCl_3$) was purchased from Acros organics. Anhydrous sodium acetate (NaOAc), ethylene glycol (EG), silver nitrate ($AgNO_3$), and sodium borohydride ($NaBH_4$) were obtained from Fisher Scientific. Sodium citrate (Na_3Cit), dopamine hydrochloride, methylene blue (MB), and rhodamine B (RhB) were purchased from Sigma-Aldrich. Ultrapure water prepared with a Millipore Milli-Q water purification system (MA, USA) was used for all experiments.

2.2. Preparation of Fe_3O_4@Polydopamine (PDA) Core−Shell Microspheres. The Fe_3O_4 microspheres were prepared with a modified solvothermal method.[23] $FeCl_3$ (2.6 g) and Na_3Cit (1.0 g) were dissolved in EG (80 mL) to form a clear solution. Afterward, NaOAc (4.0 g) was added to the mixture under stirring. After the mixture was fully dissolved, it was transferred and sealed into a Teflon-lined stainless steel autoclave. The autoclave was heated at 200 °C for 10 h and then cooled to room temperature (25 °C). The obtained black products were washed with ultrapure water and ethanol three times and then dried in vacuum at room temperature. To coat Fe_3O_4 cores with the polydopamine shell, 80 mg of Fe_3O_4 and 80 mg of dopamine hydrochloride were dissolved in 40 mL of Tris buffer solution (10 mM, pH = 8.5). After shaking for 24 h at room temperature, the products were separated and washed with ultrapure water and ethanol several times.

2.3. Preparation of Fe_3O_4@PDA-Ag Microspheres. For the preparation of Ag nanoparticles on PDA surfaces, Tollens' reagent (silver ammonia solution) was used as the Ag precursor solution. Silver ammonia solution was prepared by adding ammonia aqueous solution (2 wt %) into 10 mg mL^{-1} $AgNO_3$ solution until brown precipitation was just dissolved. An 80 mg portion of the as-prepared Fe_3O_4@PDA microspheres was added to 40 mL of silver ammonia solution, and the mixture was shaken in a rotary shaker for 12 h at room temperature. The products were collected, washed with ultrapure water and ethanol several times, and dried under vacuum. Then, Fe_3O_4@PDA-Ag-10 microspheres were obtained.

The same sample preparation procedure was carried out to obtain the Fe_3O_4@PDA-Ag-1 and Fe_3O_4@PDA-Ag-5 microspheres by using 1 and 5 mg mL^{-1} silver ammonia solution, respectively.

For comparison, $AgNO_3$ solution (10 mg mL^{-1}) was also used as the Ag source in place of silver ammonia solution following the same procedure.

2.4. Characterizations. X-ray diffraction (XRD) patterns were recorded on a Rigaku RU-200B X-ray diffractometer with a rotating anode X-ray generator and Cu Kα radiation (40 kV, 110 mA). The morphologies of microspheres were analyzed on a Philips (FEI) Morgagni 268 transmission electron microscope (TEM) operated at 80 kV and a JEOL JEM-2200FS TEM operated at 200 kV. X-ray photoelectron spectroscopy (XPS) was carried out on a Kratos Axis spectrometer with monochromatized Al Kα. The C 1s peak at 284.6 eV was used to correct all XPS spectra. The UV absorption spectra of the samples were obtained on a Thermo Scientific Evolution 300 UV−vis spectrophotometer. Zeta potentials of the microspheres were measured by using a Malvern Zetasizer Nano. Magnetic properties were examined on a Quantum Design PPMS magnetometer with an applied field between −10 000 and 10 000 Oe at room temperature.

2.5. Catalytic Reduction Experiments. A 5 mg portion of Fe_3O_4@PDA-Ag microspheres was added to 10 mL of MB aqueous solution (pH = 5.8, 40 mg L^{-1}). Subsequently, 0.5 mL of fresh $NaBH_4$ aqueous solution (0.1 mol L^{-1}) was injected into the solution under stirring. The blue color of MB gradually vanished by catalytic reduction in the presence of reducing agents. The catalytic process was monitored by measuring the changes in the absorbance at 665 nm with a UV−vis spectrophotometer. In addition, RhB was used as another model dye for catalytic reduction tests under the same procedure as MB.

2.6. Adsorption Experiments. A 5 mg portion of Fe_3O_4@PDA-Ag microspheres was added into 2 mL of MB aqueous solution (pH = 5.8, 4 mg L^{-1}) under constant stirring at room temperature. UV−vis absorption spectra of MB at different intervals were recorded to monitor the adsorption process. At the end of adsorption, the adsorbents were separated from the solution with an external magnet. The recycled adsorbents were first washed with fresh $NaBH_4$ aqueous solution (2 mL, 1.5 mmol L^{-1}) and then washed with ethanol and ultrapure water three times before the next desorption−adsorption cycle. RhB was also used as a model dye for adsorption tests under the same condition as MB.

2.7. Stability Tests. A 5 mg portion of Fe_3O_4@PDA microspheres was dispersed in 10 mL of ultrapure water and stored for half a year to test the stability of the PDA layer in aqueous solution. A 5 mg portion of Fe_3O_4@PDA-Ag-10 microspheres were dispersed in 10 mL of hydrochloric acid solution at pH 2 and pH 3 for 24 h to test the acid stability of the sample. After the stability tests, the acid solution was separated from the solid samples, and atomic absorption spectroscopy (AAS) was used to determine the concentrations of Fe^{3+}/Fe^{2+} and Ag^+ possibly present in the acid solution.

3. RESULTS AND DISCUSSIONS

3.1. Synthesis and Characterizations of Materials. Typically, Fe_3O_4 microspheres were first synthesized through a solvothermal method in ethylene glycol using anhydrous $FeCl_3$ as a single iron source. Afterward, Fe_3O_4 microspheres were mixed with dopamine solution (10 mM Tris, pH 8.5), resulting in Fe_3O_4@PDA core−shell microspheres with uniform PDA thin layers outside. Tollens' reagent (silver ammonia solution) was then added to the mixture and was *in situ* reduced by the PDA shell, leading to the deposition of Ag NPs on the shell surface (Figure 1a).

The morphology of the Fe_3O_4 core, Fe_3O_4@PDA, and Fe_3O_4@PDA-Ag-10 core−shell microspheres was characterized by TEM. The as-prepared Fe_3O_4 cores have a mean size of about 500 nm (Figure 1b). The thin PDA shell layers formed around the Fe_3O_4 cores show an average thickness of about 20 nm (Figure 1c), displaying a distinct core−shell structure. Figure 1d exhibits that the small Ag NPs (~25 nm) are densely and uniformly distributed on the PDA surface. It should be noted that modifying the concentrations of silver ammonia solution did not lead to any significant change of the size of Ag NPs (Figure S1 in the Supporting Information). The high-resolution TEM image of the Ag NPs (Figure 1e) shows that the interfringe distance of Ag NPs is measured to be 0.24 nm, which could be assigned to the {111} crystal planes of fcc Ag.[18] Furthermore, the nanobeam electron diffraction pattern (NBD) confirms the crystalline nature of metallic Ag NPs (Figure S2, Supporting Information). Figure S3a (Supporting Information) is the XRD of the obtained product. All the diffraction peaks

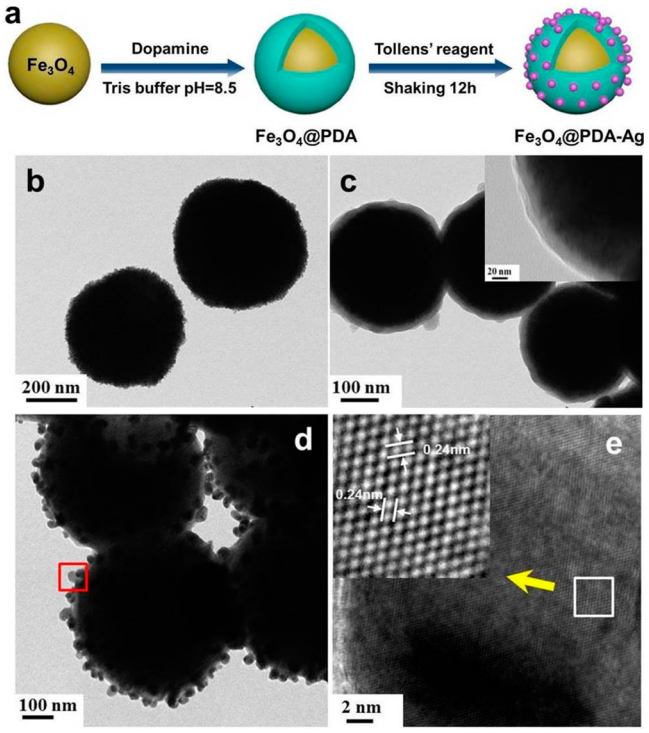

Figure 1. (a) Scheme of synthesis route of Fe_3O_4@PDA-Ag core–shell microspheres. TEM images of (b) Fe_3O_4 core microspheres and (c) Fe_3O_4@PDA core–shell microspheres. The inset is a higher-magnification image of the dopamine shell layer of Fe_3O_4@PDA core–shell microspheres. (d) Fe_3O_4@PDA-Ag-10 core–shell microspheres. (e) HRTEM image of Ag NPs enclosed by the red rectangular area in (d). The inset is the enlarged image of the white rectangular area in (e).

can be indexed to Fe_3O_4 (JCPDS 19-0629) and Ag (JCPDS 04-0783), confirming the formation of Ag NPs on the surface of Fe_3O_4@PDA particles. Figure S3b (Supporting Information) depicts the Ag 3d X-ray photoelectron spectroscopy (XPS) of Fe_3O_4@PDA-Ag. The XPS peaks at 368.1 and 374.1 eV can be assigned to Ag $3d_{5/2}$ and Ag $3d_{3/2}$, which are close to the typical binding energy of metallic Ag,[24] confirming the formation of Ag NPs at surfaces of Fe_3O_4@PDA particles. For comparison, $AgNO_3$ solution was also used as the Ag source for the deposition of Ag NPs. Figure S4 (Supporting Information) reveals the low loading amount and large size of the obtained Ag NPs.

Figure 2 shows the magnetic hysteresis loop of Fe_3O_4@PDA-Ag-10 core–shell microspheres at room temperature. The saturation magnetization value (M_s) was measured to be 45.5 emu g^{-1}. It should be noted that almost no hysteresis loops were found in the magnetization curve, suggesting the superparamagnetism of Fe_3O_4@PDA-Ag-10 core–shell microspheres. Owing to the high magnetization values and superparamagnetic characteristics, the Fe_3O_4@PDA-Ag-10 core–shell microspheres can be magnetically separated from aqueous solution within a few seconds and redispersed well once the magnet is removed, rendering them economic and reusable for various applications (see the video in the Supporting Information).

3.2. Catalytic Reduction Tests. It has been long identified that Ag NPs show excellent catalytic activity and selectivity on many catalytic reactions.[25,26] Herein, the catalytic reduction of MB by $NaBH_4$ was used as a model reaction to investigate the

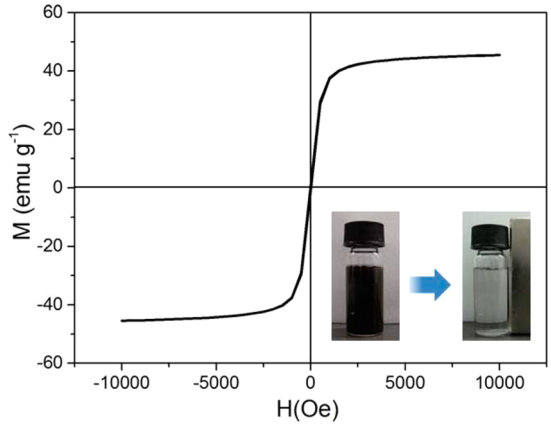

Figure 2. Magnetic hysteresis loop of Fe_3O_4@PDA-Ag-10 microspheres. The inset photographs: separation of Fe_3O_4@PDA-Ag-10 microspheres from aqueous dispersion using an external magnet.

catalytic performance of Fe_3O_4@PDA-Ag-10 core–shell microspheres This reaction can be monitored by the color bleaching of MB solution after the addition of the catalysts and an excess amount of $NaBH_4$, as indicated by the gradual decrease in the maximum absorbance values (λ_{max} = 665 nm) with time in the UV–vis spectra. As shown in Figure 3a, the adsorption peak at λ_{max} gradually decreases with respect to reaction time, indicating the reduction of MB by Fe_3O_4@PDA-Ag. To clarify the catalytic effect of Ag NPs, a control experiment was conducted by using Fe_3O_4@PDA as the catalysts. To elucidate the reaction mechanism, the concentration of $NaBH_4$ could be considered as constant throughout the reaction since it was in a great excess (0.1 M). Therefore, pseudo-first-order kinetics with regard to the catalytic reduction of MB, described as $\ln(C_t/C_0) = -kt$, can be applied, where C_t is the concentration of MB at time t, C_0 is the initial concentration of MB, and k is the rate constant.[27] Figure 3b reveals the linear relationship between $\ln(C_t/C_0)$ and the reaction time t (C_0 = 40 mg L^{-1}, V_{MB} = 10 mL). The rate constant k of MB catalytic reduction is calculated to be 0.430 min^{-1} at 25 °C for the case with Fe_3O_4@PDA-Ag-10 core–shell microspheres, whereas, as expected, Fe_3O_4@PDA has little catalytic activity with a rate constant of 0.005 min^{-1} (Figure 3b). When the initial amount of MB solution was reduced to half (i.e., 5 mL), the reaction could be quickly completed within 20 s with the same amount of catalyst and $NaBH_4$ (Figure 3c). It should be noted that, despite the comparatively higher concentration of MB solution (C_0 = 40 mg L^{-1}) used in the current work, the bleaching rate is considerably higher than the rates reported previously under similar experimental conditions with Ag NPs.[20,21] This outstanding catalytic performance could be ascribed to the relatively smaller size and higher loading amount of Ag nanoparticles in our developed Fe_3O_4@PDA-Ag-10 core–shell microspheres. By delicately choosing $AgNO_3$ as the Ag source, the Fe_3O_4@PDA-Ag microspheres with larger sizes of Ag NPs were prepared (TEM images shown in Figure S4, Supporting Information). Compared with Fe_3O_4@PDA-Ag-10 using silver ammonia as the Ag source (Figure 3c), it shows relatively lower catalytic activity (Figure 3d) mainly due to the decrease of active sites for catalytic reaction on larger Ag NPs. To investigate the impact of the content of Ag NPs on the catalytic activity of Fe_3O_4@PDA-Ag, two lower concentrations of silver ammonia solution (1 and 5 mg mL^{-1}) were used to prepare Fe_3O_4@PDA-Ag-1 and Fe_3O_4@PDA-Ag-5, respectively. It

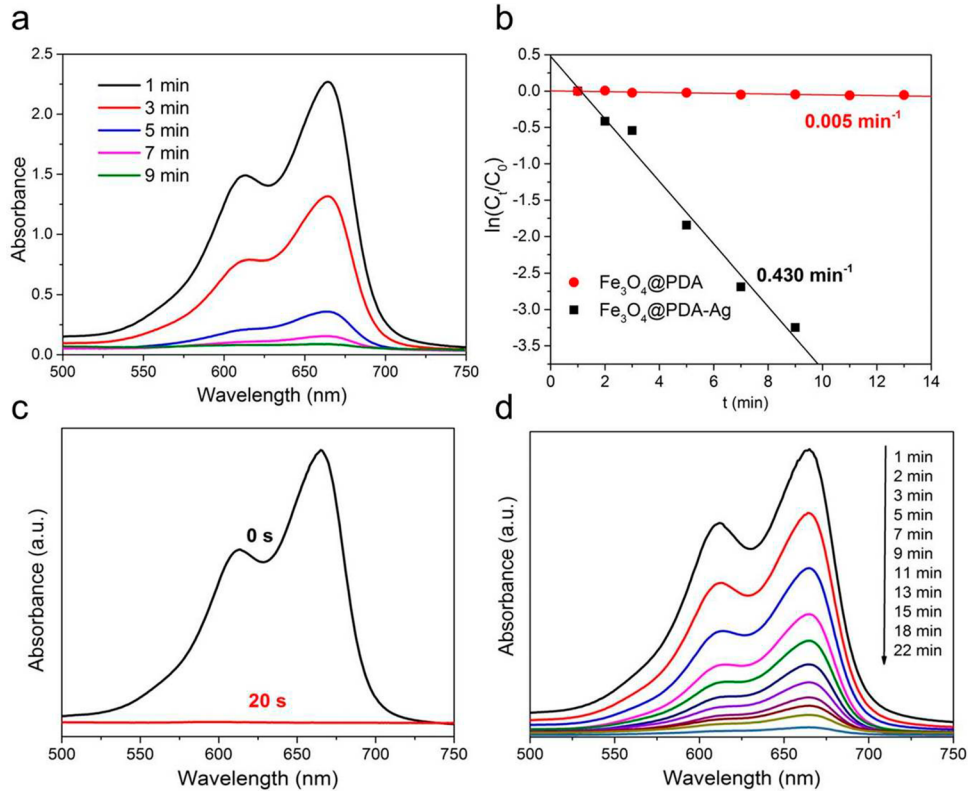

Figure 3. (a) Successive UV−vis spectra for catalytic reduction of MB aqueous solution (40 mg L^{-1}) by $NaBH_4$ and Fe_3O_4@PDA-Ag-10 core−shell microspheres. (b) First-order kinetics plot of catalytic reduction of MB in the presence of Fe_3O_4@PDA and Fe_3O_4@PDA-Ag-10 core−shell microspheres. Successive UV−vis spectra for MB (40 mg L^{-1}) catalytic reduction by $NaBH_4$ and Fe_3O_4@PDA-Ag core−shell microspheres prepared by using (c) 10 mg mL^{-1} silver ammonia solution and (d) 10 mg mL^{-1} $AgNO_3$ as the Ag source, respectively.

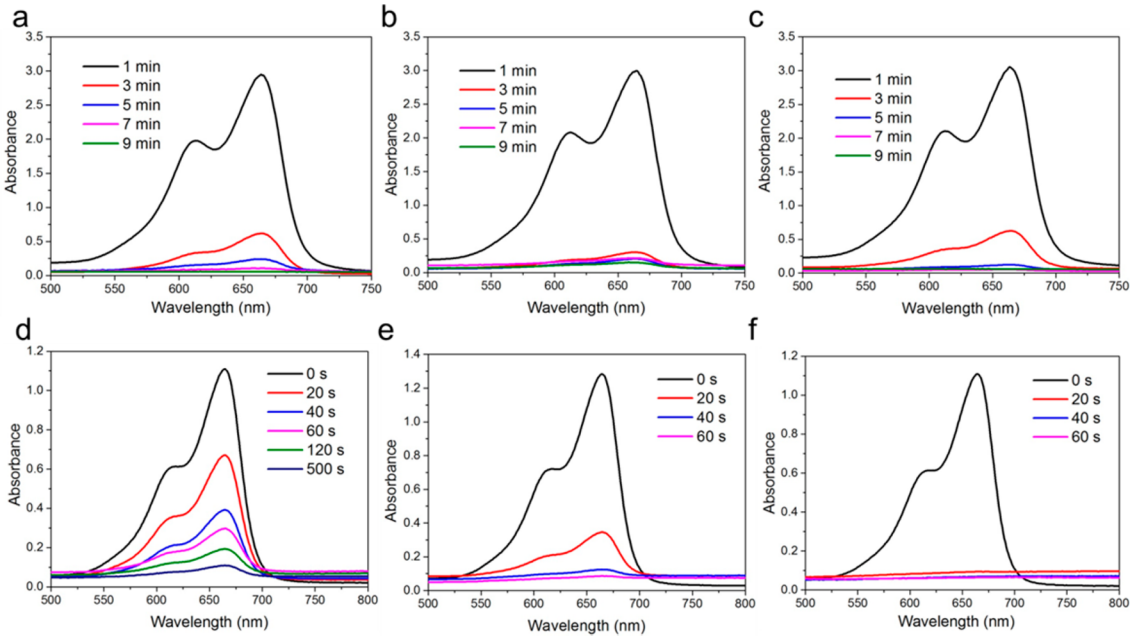

Figure 4. Successive UV−vis spectra for catalytic reduction of MB aqueous solution (40 mg L^{-1}) by $NaBH_4$ and Fe_3O_4@PDA-Ag-10 core−shell microspheres at (a) pH 3, (b) pH 7, and (c) pH 9. Successive UV−vis spectra for the adsorption of MB aqueous solution (4 mg L^{-1}) by Fe_3O_4@PDA-Ag-10 core−shell microspheres at (d) pH 3, (e) pH 7, and (f) pH 9.

should be noted that increasing the concentrations of silver ammonia solution did not lead to significant change in the size of Ag NPs but could enhance the loading content of Ag NPs (Figure S1, Supporting Information), resulting in better catalytic performance as shown in Figure S5 (Supporting Information).

To evaluate the pH effect of the MB solution on the catalytic activity of Fe_3O_4@PDA-Ag-10 microspheres, MB solutions

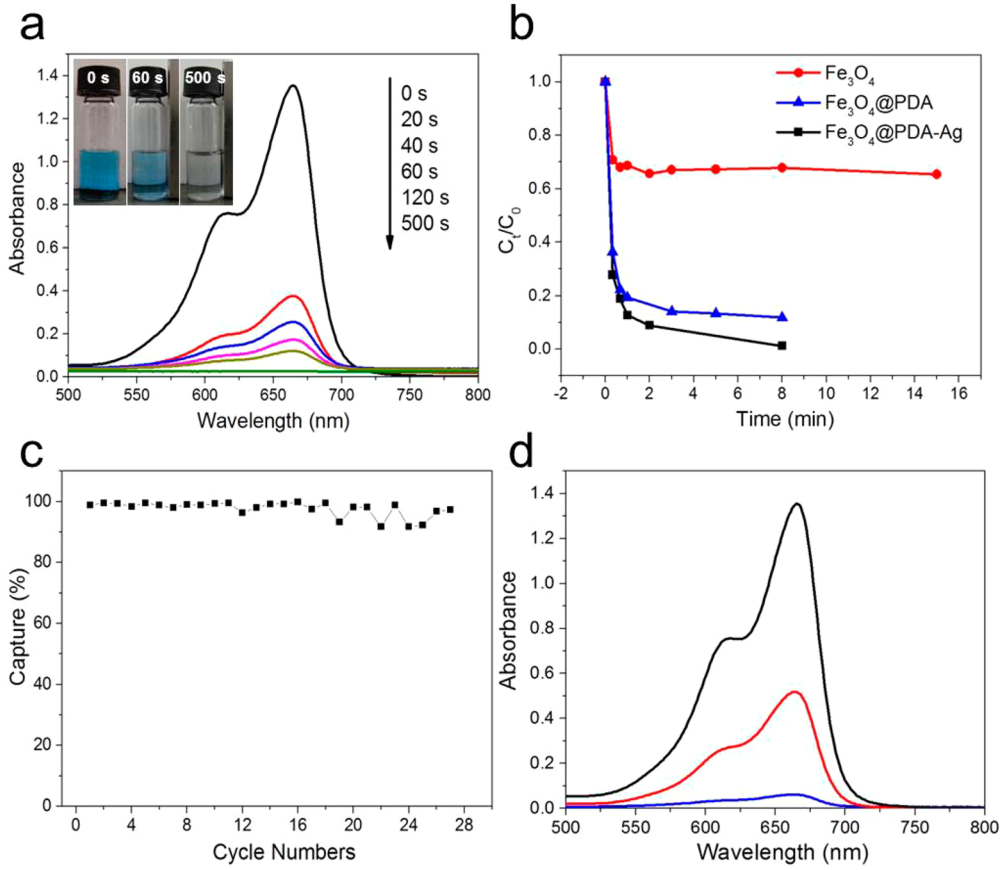

Figure 5. (a) Successive UV−vis absorption spectra of MB aqueous solution (4 mg L^{-1}) in the presence of Fe_3O_4@PDA-Ag-10 core−shell microspheres. (b) Adsorption rate curves of MB after the addition of different adsorbents. (c) The recyclability of Fe_3O_4@PDA-Ag-10 microspheres for the adsorption of MB. (d) UV−vis adsorption spectra of MB solution in the presence of adsorbents regenerated with different desorption agents after one cycle: $NaBH_4$ solution first, and then water and ethanol (blue curve), only with water and ethanol (red curve), and initial MB solution (black curve). Inset in (a) shows the color change of MB solution with time after the addition of Fe_3O_4@PDA-Ag-10 microspheres.

with three different pH values (pH 3, 7, 9) were used for the tests. Figure 4a−c shows that there is no significant change on the catalytic activity of Fe_3O_4@PDA-Ag-10 under different pH conditions, which implies that the high catalytic activity of the microspheres could withhold in various solution conditions of different pHs.

Additionally, the catalytic activity of Fe_3O_4@PDA-Ag-10 microspheres on another model organic dye, RhB, was also tested. Figure S6 (Supporting Information) reveals that the maximum absorbance value at λ_{max} = 554 nm of RhB decreases with reaction time, which demonstrates that Fe_3O_4@PDA-Ag is also able to catalyze the reduction of RhB with $NaBH_4$. The catalytic reaction could be completed within 9 min, as efficient as a previous report employing Ag/SBA-15 as the catalyst[26] despite the comparatively higher concentration of RhB solution in this work. Therefore, the Fe_3O_4@PDA-Ag core−shell microspheres exhibit the potential application as an effective catalyst for the reduction of various organic dyes.

The above results reveal the high catalytic performance of Fe_3O_4@PDA-Ag core−shell microspheres, which are most likely attributed to the strong binding between the PDA layer and the Ag NPs due to the strong metal coordination ability of the catechol groups in the PDA layer.[19,28,29]

3.3. Adsorption Tests. Another interesting feature of an Fe_3O_4@PDA-Ag microsphere is that it shows efficient adsorption of organic dyes in addition to the high catalytic activity. Again, MB was chosen as a model dye for the adsorption test. UV−vis spectroscopy was applied to monitor the adsorption process of MB after adding Fe_3O_4@PDA-Ag-10 core−shell microspheres under stirring at ambient temperature. As shown in Figure 5a, the intensity of the adsorption peak at λ_{max} dropped drastically within 20 s after the adsorbents were added, and the adsorption peak finally vanished after 500 s, indicating their rapid adsorption of MB. Figure 5b demonstrates that the adsorption performance of Fe_3O_4@PDA is similar to that of Fe_3O_4@PDA-Ag-10, whereas Fe_3O_4 shows much lower adsorption capability. Consequently, the remarkable adsorption rate can be ascribed to the presence of the PDA layer. Because of the well-known reducing ability of PDA to many metallic ions,[15,16,19,20] a control experiment was carried out to rule out the possibility of the reduction of MB by the PDA layer. The UV−vis spectra of the resultant solution after adsorption by Fe_3O_4@PDA microspheres and the catalytic reduction product catalyzed by Fe_3O_4@PDA-Ag microspheres were examined. The results are shown in Figure S7 (Supporting Information), from which it was found that the catalytic reduction product (leucomethylene blue) exhibits a very strong UV−vis absorption peak at 256 nm, indicating the characteristic aromatic structure of the reduced MB,[30−32] whereas the UV−vis spectra of the solution after adsorption exhibit no absorption peak at 256 nm. Additionally, the Fe_3O_4@PDA-Ag-10 microspheres also exhibit some adsorption behavior on RhB with a removal efficiency of ∼50% in less than 10 min, as shown in Figure S8 (Supporting Information).

dx.doi.org/10.1021/am501632f | ACS Appl. Mater. Interfaces 2014, 6, 8845−8852

The possible adsorption mechanism could be the synergistic effects of electrostatic interaction, $\pi-\pi$ interaction, and hydrogen bonding between PDA layers and organic dyes.[12] The zeta potential of Fe_3O_4@PDA-Ag-10 at pH 5.8 was determined to be about −45 mV (Figure S9, Supporting Information), suggesting strong electrostatic interactions with positively charged MB (Figure S10, Supporting Information). To confirm the presence of electrostatic interactions between the PDA layer and MB, the effect of pH on the adsorption behavior of Fe_3O_4@PDA-Ag-10 was investigated. Although it was found that the catalytic activity of Fe_3O_4@PDA-Ag-10 microspheres does not change with pH, the adsorption performance of the microspheres improves with increasing solution pH (Figure 4d−f). Figure 4d−f shows that the Fe_3O_4@PDA-Ag-10 microspheres adsorb MB faster at higher pH, which is most likely attributed to the stronger electrostatic interactions between the microspheres and MB under higher pH, as confirmed by zeta potential measurement of Fe_3O_4@PDA-Ag-10, which becomes more negatively charged at higher pH (Figure S9). According to the previous results, the magnetically separable Fe_3O_4@PDA-Ag microspheres can be used as a kind of promising efficient adsorbent in wastewater treatment.

The recyclability of the adsorbents was also evaluated. Figure 4c shows that the Fe_3O_4@PDA-Ag microspheres could be recycled and reused for at least 27 times with a stable adsorption of more than 90%, which is better than the recycle performance of Fe_3O_4@C nanocomposites[27] and graphene or graphene oxide based hydrogels.[5,12] Moreover, the recycle process of the novel Fe_3O_4@PDA-Ag materials can be completed in several minutes, faster than the regeneration of hydrogel reported previously, which typically lasts more than 30 min.[12,21]

According to the UV−vis absorption spectra of Figure 5d, it should be also noted that only 60% of the adsorbed MB can be removed from the adsorbents under the conventional regeneration procedure (viz. using water and ethanol), as compared with almost 100% removal by the addition of small amounts (2 mL) of $NaBH_4$ solution (1.5 mM) ahead of water and ethanol. The removal efficiency is described as $X\% = 1 - C_t/C_0 = 1 - I_t/I_0$, where $X\%$ is the removal efficiency on MB, C_0 and C_t are the concentrations of MB before and after adsorption by Fe_3O_4@PDA-Ag, respectively, and I_0 and I_t are the intensities of the absorption peak at 665 nm of MB before and after adsorption by Fe_3O_4@PDA-Ag, respectively. The addition of a small amount of $NaBH_4$ can significantly facilitate the removal of MB on Fe_3O_4@PDA-Ag microspheres via a catalytic process, in which the Fe_3O_4@PDA-Ag microspheres perform as an electron relay system.[33,34] Firstly, $NaBH_4$ and MB were adsorbed onto the surface of Ag NPs to initiate the catalytic reaction. When the reaction was over, the reduced MB (viz. leucomethylene blue, $pK_a = 5.8$[30]) could be spontaneously desorbed or removed from the surface of Ag NPs and diffused into the solution due to decreased electrostatic interactions between PDA layers and reduced MB after adding $NaBH_4$ solution (pH 9.4).[27,35] Therefore, the reduced MB could be easily washed away by the addition of ethanol and water consequentially. The presence of reduced MB solution in the catalytic reduction could be confirmed by the forementioned UV−vis spectra (Figure S7, Supporting Information). The UV−vis spectra of the catalytic reduction product exhibits a characteristic absorption peak at 256 nm, which corresponds to the aromatic structure of the reduced MB.[30−32] The whole regeneration process is time-efficient (~6 min), and the adsorbents can be easily separated from the reduced MB solution under an external magnetic field (see the video in the Supporting Information). The excellent recyclability and efficient regeneration of the adsorbents might be attributed to the stabilizations of the Ag NPs by PDA layers, which prevent reduction in activity due to the coagulation of Ag NPs.[15] Our results suggest that the Fe_3O_4@PDA-Ag materials could be more favorable for practical use in wastewater treatment over conventional adsorbents in terms of long reusability and fast regeneration rate.

3.4. Stability Tests. The good stability of Fe_3O_4@PDA-Ag microspheres is a critical factor for their practical applications. There are two possibilities that will influence the stability of our developed materials: degradability of PDA layers in the aqueous solution and acid etching of Fe_3O_4. In this work, the long-term stability of PDA films in aqueous solution was first investigated. As shown in Figure 6a, even after half a year of soaking in aqueous solution, the distinct PDA layers were still stably coated on the Fe_3O_4 cores with a thickness of ~20 nm and the same morphology as the fresh Fe_3O_4@PDA samples shown in Figure 1c, indicating the good stability of the PDA layer in an aqueous environment over a reasonably long period of time. Meanwhile, due to the fact that Fe_3O_4 microspheres could be easily etched under acid conditions, the acid stability of Fe_3O_4@PDA-Ag-10 was also tested under a strong acid environment (pH 2 and pH 3) for over 24 h. The TEM images (Figure 6b,c) show that the Fe_3O_4@PDA-Ag-10 microspheres still maintain the core−shell structure under the strong acid conditions. Furthermore, the AAS results (Table 1) confirm that the Fe_3O_4@PDA-Ag-10 can withstand the strong acid condition, and there were only about 1% (w/w) of the leakage of Fe^{3+}/Fe^{2+} and almost no leakage of Ag^+ into the solution over 24 h. Therefore, the robust PDA layer could effectively protect the Fe_3O_4 cores and bind the Ag NPs under strong acid conditions and show good stability in practical applications.

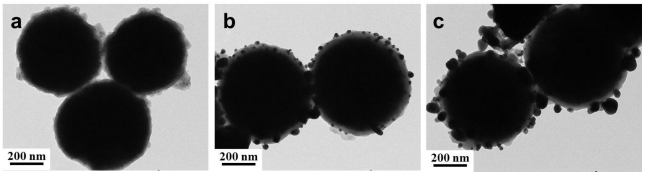

Figure 6. TEM images of (a) Fe_3O_4@PDA microspheres dispersed in aqueous solution for half a year, (b) Fe_3O_4@PDA-Ag-10 microspheres dispersed in acid solution with pH 2 for 24 h, and (c) Fe_3O_4@PDA-Ag-10 microspheres dispersed in acid solution with pH 3 for 24 h.

4. CONCLUSION

In conclusion, a facile, *in situ*, and efficient approach was demonstrated for the preparation of Fe_3O_4@PDA-Ag core−shell microspheres. These Ag-immobilized microspheres show excellent catalytic capabilities on the reduction of a model organic dye MB with $NaBH_4$ as well as fast adsorption/removal rate of MB from aqueous solutions at different pH values. The remarkable catalytic reduction and adsorption performance can be attributed to the monodisperse Ag NPs and mussel-inspired PDA layers coated on the magnetic microspheres. More importantly, the as-prepared Fe_3O_4@PDA-Ag microspheres exhibit excellent reusability for at least 27 cycles and fast

Table 1. AAS Results of Fe_3O_4@PDA-Ag-10 Microspheres under Acid Conditions

sample name	pH	$C_{Fe^{3+}/Fe^{2+}}$ (mg/L)	C_{Ag^+} (mg/L)	$W_{Fe^{3+}/Fe^{2+}}/W_{sample}$ (%)	W_{Ag^+}/W_{sample} (%)
Fe_3O_4@PDA-Ag-10	2	5.53	0.07	1.1	0.014
Fe_3O_4@PDA-Ag-10	3	4.47	0.07	0.89	0.014

regeneration by using $NaBH_4$ via a unique desorption mechanism of the catalytic process. The superparamagnetic properties of the Fe_3O_4@PDA-Ag microspheres enable them to be easily recovered for reuse under an external magnetic field. Additionally, the Fe_3O_4@PDA-Ag microspheres possess good stability under strong acid conditions and can keep in the aqueous solution over long periods of time. The versatile mussel-inspired PDA polymer coatings on the Fe_3O_4@PDA-Ag microspheres also allow the further surface functionalization for the development of multifunctional adsorbent materials. Our results suggest that the Fe_3O_4@PDA-Ag materials developed have great potential applications in catalysis and wastewater treatment.

■ ASSOCIATED CONTENT

Supporting Information

XRD patterns, Ag 3d XPS spectra, TEM images, additional UV−vis spectra for MB, molecular structure of MB, zeta potentials of the sample. This material is available free of charge via the Internet at http://pubs.acs.org.

■ AUTHOR INFORMATION

Corresponding Authors

*E-mail: hongbo.zeng@ualberta.ca. Phone: 780-492-1044. Fax: 780-492-2881 (H. Z.).

*E-mail: yhdeng@scut.edu.cn (Y.D.).

Author Contributions

⊥All authors have given approval to the final version of the manuscript. Y.X. and B.Y. contributed equally to this work.

Notes

The authors declare no competing financial interest.

■ ACKNOWLEDGMENTS

The authors are grateful for the financial support from the Natural Sciences and Engineering Research Council of Canada (NSERC), the Helmholtz-Alberta Initiative − Energy & Environment (HAI-E&E) program, and the Australian Research Council (DE 120100042). The authors also acknowledge the Alberta Centre for Surface Engineering and Science (ACSES) and the National Institute for Nanotechnology (NINT) for the materials characterization.

■ REFERENCES

(1) Wang, P.; Shi, Q.; Shi, Y.; Clark, K. K.; Stucky, G. D.; Keller, A. A. Magnetic Permanently Confined Micelle Arrays for Treating Hydrophobic Organic Compound Contamination. *J. Am. Chem. Soc.* **2008**, *131*, 182−188.

(2) Sui, Z.; Meng, Q.; Zhang, X.; Ma, R.; Cao, B. Green Synthesis of Carbon Nanotube-Graphene Hybrid Aerogels and Their Use as Versatile Agents for Water Purification. *J. Mater. Chem.* **2012**, *22*, 8767−8771.

(3) Yu, K.; Yang, S.; Liu, C.; Chen, H.; Li, H.; Sun, C.; Boyd, S. A. Degradation of Organic Dyes via Bismuth Silver Oxide Initiated Direct Oxidation Coupled with Sodium Bismuthate Based Visible Light Photocatalysis. *Environ. Sci. Technol.* **2012**, *46*, 7318−7326.

(4) Ali, I. New Generation Adsorbents for Water Treatment. *Chem. Rev.* **2012**, *112*, 5073−5091.

(5) Tiwari, J. N.; Mahesh, K.; Le, N. H.; Kemp, K. C.; Timilsina, R.; Tiwari, R. N.; Kim, K. S. Reduced Graphene Oxide-Based Hydrogels for the Efficient Capture of Dye Pollutants from Aqueous Solutions. *Carbon* **2013**, *56*, 173−182.

(6) Zhu, T.; Chen, J. S.; Lou, X. W. Highly Efficient Removal of Organic Dyes from Waste Water Using Hierarchical NiO Spheres with High Surface Area. *J. Phys. Chem. C* **2012**, *116*, 6873−6878.

(7) Panizza, M.; Cerisola, G. Direct and Mediated Anodic Oxidation of Organic Pollutants. *Chem. Rev.* **2009**, *109*, 6541−6569.

(8) Moussavi, G.; Mahmoudi, M. Removal of Azo and Anthraquinone Reactive Dyes from Industrial Wastewaters Using MgO Nanoparticles. *J. Hazard. Mater.* **2009**, *168*, 806−812.

(9) Wu, J.; Wang, J.; Li, H.; Du, Y.; Huang, K.; Liu, B. Designed Synthesis of Hematite-Based Nanosorbents for Dye Removal. *J. Mater. Chem. A* **2013**, *1*, 9837−9847.

(10) Meshko, V.; Markovska, L.; Mincheva, M.; Rodrigues, A. E. Adsorption of Basic Dyes on Granular Acivated Carbon and Natural Zeolite. *Water Res.* **2001**, *35*, 3357−3366.

(11) Yan, Y.; Zhang, M.; Gong, K.; Su, L.; Guo, Z.; Mao, L. Adsorption of Methylene Blue Dye onto Carbon Nanotubes: A Route to an Electrochemically Functional Nanostructure and Its Layer-by-Layer Assembled Nanocomposite. *Chem. Mater.* **2005**, *17*, 3457−3463.

(12) Gao, H.; Sun, Y.; Zhou, J.; Xu, R.; Duan, H. Mussel-Inspired Synthesis of Polydopamine-Functionalized Graphene Hydrogel as Reusable Adsorbents for Water Purification. *ACS Appl. Mater. Interfaces* **2012**, *5*, 425−432.

(13) Bandara, N.; Zeng, H.; Wu, J. Marine Mussel Adhesion: Biochemistry, Mechanisms, and Biomimetics. *J. Adhes. Sci. Technol.* **2012**, *27*, 2139−2162.

(14) Zeng, H.; Hwang, D. S.; Israelachvili, J. N.; Waite, J. H. Strong Reversible Fe^{3+}-Mediated Bridging between Dopa-Containing Protein Films in Water. *Proc. Natl. Acad. Sci. U.S.A.* **2010**, *107*, 12850−12853.

(15) Liu, R.; Guo, Y.; Odusote, G.; Qu, F.; Priestley, R. D. Core−Shell Fe_3O_4 Polydopamine Nanoparticles Serve Multipurpose as Drug Carrier, Catalyst Support and Carbon Adsorbent. *ACS Appl. Mater. Interfaces* **2013**, *5*, 9167−9171.

(16) Lee, H.; Dellatore, S. M.; Miller, W. M.; Messersmith, P. B. Mussel-Inspired Surface Chemistry for Multifunctional Coatings. *Science* **2007**, *318*, 426−430.

(17) Zhang, M.; He, X.; Chen, L.; Zhang, Y. Preparation of IDA-Cu Functionalized Core-Satellite Fe_3O_4/Polydopamine/Au Magnetic Nanocomposites and Their Application for Depletion of Abundant Protein in Bovine Blood. *J. Mater. Chem.* **2010**, *20*, 10696−10704.

(18) Jeon, E. K.; Seo, E.; Lee, E.; Lee, W.; Um, M.-K.; Kim, B.-S. Mussel-Inspired Green Synthesis of Silver Nanoparticles on Graphene Oxide Nanosheets for Enhanced Catalytic Applications. *Chem. Commun.* **2013**, *49*, 3392−3394.

(19) Guo, L.; Liu, Q.; Li, G.; Shi, J.; Liu, J.; Wang, T.; Jiang, G. A Mussel-Inspired Polydopamine Coating as a Versatile Platform for the in Situ Synthesis of Graphene-Based Nanocomposites. *Nanoscale* **2012**, *4*, 5864−5867.

(20) Sureshkumar, M.; Lee, P.-N.; Lee, C.-K. Stepwise Assembly of Multimetallic Nanoparticles via Self-Polymerized Polydopamine. *J. Mater. Chem.* **2011**, *21*, 12316−12320.

(21) Zheng, Y.; Wang, A. Ag Nanoparticle-Entrapped Hydrogel as Promising Material for Catalytic Reduction of Organic Dyes. *J. Mater. Chem.* **2012**, *22*, 16552−16559.

(22) Nadagouda, M. N.; Desai, I.; Cruz, C.; Yang, D. J. Novel Pd Based Catalyst for the Removal of Organic and Emerging Contaminants. *RSC Adv.* **2012**, *2*, 7540−7548.

(23) Liu, J.; Sun, Z.; Deng, Y.; Zou, Y.; Li, C.; Guo, X.; Xiong, L.; Gao, Y.; Li, F.; Zhao, D. Highly Water-Dispersible Biocompatible

Magnetite Particles with Low Cytotoxicity Stabilized by Citrate Groups. *Angew. Chem., Int. Ed.* **2009**, *48*, 5875−5879.
(24) Guo, X.; Zhang, Q.; Sun, Y.; Zhao, Q.; Yang, J. Lateral Etching of Core−Shell Au@Metal Nanorods to Metal-Tipped Au Nanorods with Improved Catalytic Activity. *ACS Nano* **2012**, *6*, 1165−1175.
(25) Patel, A. C.; Li, S.; Wang, C.; Zhang, W.; Wei, Y. Electrospinning of Porous Silica Nanofibers Containing Silver Nanoparticles for Catalytic Applications. *Chem. Mater.* **2007**, *19*, 1231−1238.
(26) Chi, Y.; Zhao, L.; Yuan, Q.; Li, Y.; Zhang, J.; Tu, J.; Li, N.; Li, X. Facile Encapsulation of Monodispersed Silver Nanoparticles in Mesoporous Compounds. *Chem. Eng. J.* **2012**, *195−196*, 254−260.
(27) Zhu, M.; Wang, C.; Meng, D.; Diao, G. In Situ Synthesis of Silver Nanostructures on Magnetic Fe_3O_4@C Core−Shell Nanocomposites and Their Application in Catalytic Reduction Reactions. *J. Mater. Chem. A* **2013**, *1*, 2118−2125.
(28) Zhang, M.; Zheng, J.; Zheng, Y.; Xu, J.; He, X.; Chen, L.; Fang, Q. Preparation, Characterization and Catalytic Activity of Core−Satellite Au/Pdop/SiO_2/Fe_3O_4 Magnetic Nanocomposites. *RSC Adv.* **2013**, *3*, 13818−13824.
(29) Ryu, J.; Ku, S. H.; Lee, H.; Park, C. B. Mussel-Inspired Polydopamine Coating as a Universal Route to Hydroxyapatite Crystallization. *Adv. Funct. Mater.* **2010**, *20*, 2132−2139.
(30) Impert, O.; Katafias, A.; Kita, P.; Mills, A.; Pietkiewicz-Graczyk, A.; Wrzeszcz, G. Kinetics and Mechanism of a Fast Leuco-Methylene Blue Oxidation by Copper(II)-Halide Species in Acidic Aqueous Media. *Dalton Trans.* **2003**, 348−353.
(31) Jiang, Y.; Zhang, S.; Ji, Q.; Zhang, J.; Zhang, Z.; Wang, Z. Ultrathin Cu_7S_4 Nanosheets-Constructed Hierarchical Hollow Cubic Cages: One-Step Synthesis Based on Kirkendall Effect and Catalysis Property. *J. Mater. Chem. A* **2014**, *2*, 4574−4579.
(32) Ray, C.; Dutta, S.; Sarkar, S.; Sahoo, R.; Roy, A.; Pal, T. A Facile Synthesis of 1D Nano Structured Selenium and Au Decorated Nano Selenium: Catalysts for the Clock Reaction. *RSC Adv.* **2013**, *3*, 24313−24320.
(33) Jana, N. R.; Sau, T. K.; Pal, T. Growing Small Silver Particle as Redox Catalyst. *J. Phys. Chem. B* **1998**, *103*, 115−121.
(34) Mallick, K.; Witcomb, M.; Scurrell, M. Silver Nanoparticle Catalysed Redox Reaction: An Electron Relay Effect. *Mater. Chem. Phys.* **2006**, *97*, 283−287.
(35) Jiang, Z.-J.; Liu, C.-Y.; Sun, L.-W. Catalytic Properties of Silver Nanoparticles Supported on Silica Spheres. *J. Phys. Chem. B* **2005**, *109*, 1730−1735.